

Use of the Differential Charging Effect in XPS to Determine the Nature of Surface Compounds Resulting from the Interaction of a Pt/(BaCO₃ + CeO₂) Model Catalyst with SO_x

M. Yu. Smirnov^a, A. V. Kalinkin^a, A. A. Dubkov^b, E. I. Vovk^a, A. M. Sorokin^a,
A. I. Nizovskii^a, B. Carberry^b, and V. I. Bukhtiyarov^{a, c}

^a Boreskov Institute of Catalysis, Siberian Branch, Russian Academy of Sciences, Novosibirsk, 630090 Russia

^b Ford Forschungszentrum Aachen GmbH, Aachen, D-52072 Germany

^c Novosibirsk State University, Novosibirsk, 630090 Russia

e-mail: smirnov@catalysis.ru

Received November 9, 2010

Abstract—Changes in the chemical composition of the surface of a Pt/(BaCO₃ + CeO₂) model NO_x storage–reduction catalyst upon its interaction with SO_x (SO₂ (260 Pa) + O₂ (2600 Pa) + H₂O (525 Pa)) followed by regeneration in a mixture of CO (2100 Pa) with H₂O (525 Pa) were studied by X-ray photoelectron spectroscopy (XPS). Model catalyst samples were prepared as a thin film (about several hundreds of angstrom units in thickness) on the surface of tantalum foil coated with a layer of aluminum oxide (~100 Å). It was found that the Pt/BaCO₃ and Pt/CeO₂ catalyst constituents acquired different surface charges (differential charging) in the course of photoelectron emission; because of this, it was possible to determine the nature of surface compounds formed as a result of the interaction of the catalyst with a reaction atmosphere. It was found that barium carbonate was converted into barium sulfate as a result of reaction with SO_x on the surface of BaCO₃ at 150°C. As the treatment temperature in SO_x was increased to 300°C, the formation of sulfate on the surface of CeO₂ was observed. The sulfatization of CeO₂ was accompanied by the reduction of Ce(IV) to Ce(III). The regeneration reaction of the catalyst treated in SO_x at 300°C resulted in the consecutive decomposition of cerium(III) sulfate at ≤500°C and then barium sulfate at 600–700°C. Upon the decomposition of BaSO₄, a portion of sulfur was converted into a sulfide state, probably, because of the formation of BaS.

DOI: 10.1134/S0023158411040161

INTRODUCTION

The current development of automobile industry is oriented toward decreasing fuel consumption and reducing carbon dioxide emissions into the atmosphere. In particular, this can be achieved by the use of engines with a lean air–fuel mixture. However, under these conditions, nitrogen oxides are formed in considerable amounts, and they cannot be efficiently neutralized on commonly used three-way catalysts with a large excess of oxygen in the reaction mixture. Toyota developed so-called NO_x storage–reduction (NSR) catalysts [1] as an approach to solve the problem of the neutralization of nitrogen oxides. The principle of operation of the NSR catalyst is the following: the basic component of the catalyst binds nitrogen oxides as nitrates in contact with NO_x in an oxidizing atmosphere; then, nitrates are reduced to nitrogen during a short pulse injection of an excess of fuel, which increases the amount of reducing gases (CO, H₂, and CH_x) in the exhaust [1, 2]. Traditionally, Ba-containing substances—BaO, Ba(OH)₂, and BaCO₃—supported on γ-Al₂O₃ are used as the basic components of the NSR catalyst. Platinum is introduced into the catalyst for the more efficient oxidation of NO to NO₂.

and then to barium nitrate under oxidizing conditions and for the subsequent nitrate reduction to nitrogen under reducing conditions.

A disadvantage of NSR catalysts of this type is their high sensitivity to poisoning by sulfur compounds, which appear in exhaust gases as a result of the oxidation of S-containing impurities in fuel. It was found that the interaction of a catalyst with sulfur oxides in an oxidizing atmosphere leads to the formation of stable barium sulfates, as a result of which the absorption capacity for nitrogen oxides decreases [3–11]. Catalyst regeneration, which consists in the removal of the sulfate ion, is performed in a reducing atmosphere at high temperatures, which are reached by the short-term injection of an additional amount of fuel. At the same time, high-temperature regeneration can cause undesirable changes in the state of the catalyst, such as a decrease in the specific surface area, the agglomeration of platinum, and the formation of barium aluminates, which are inert with respect to the absorption of NO_x [8]. The formation of barium sulfides [8, 10, 12, 13] and/or platinum sulfides [4, 10, 14, 15] is also possible; it also leads to a decrease in the catalyst activity.

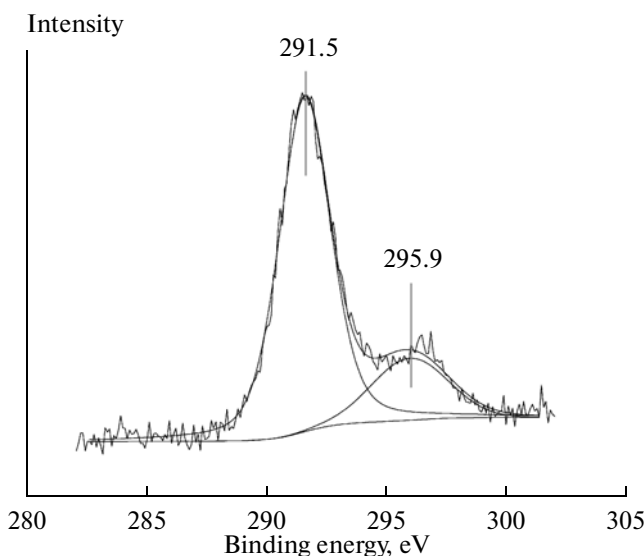


Fig. 1. XPS spectrum of the Pt/(BaCO₃ + CeO₂) model catalyst in the initial state measured in the C 1s region with no correction for charging and no background subtraction.

A method for increasing the resistance of NSR catalysts to poisoning by sulfur-containing impurities is the introduction of CeO₂, TiO₂, Fe₂O₃, and MgO additives into the catalysts [16–20] or the replacement of an Al₂O₃ support by an oxide less prone to the formation of sulfates [21, 22]. It was shown that, in the operation of a catalyst containing cerium dioxide along with a BaO (BaCO₃) basic component, a portion of SO_x was bound to the catalyst as cerium sulfate. Thus, the fraction of the Ba-containing component, which was eliminated from the process of NO_x removal as a result of conversion into barium sulfate, decreased [16]. It is assumed that cerium dioxide also plays a positive role in the regeneration of an NSR catalyst because of its high catalytic activity in the reaction of water gas conversion with the formation of H₂ [23].

In this work, we report the results of a study of the interaction of SO_x with the samples of a model NSR catalyst containing Pt, BaCO₃, and CeO₂ performed by X-ray photoelectron spectroscopy (XPS). The aim of this study was to determine the nature of the resulting surface compounds and the conditions of sulfate formation and decomposition on the surfaces of BaCO₃ and CeO₂. We used XPS because this technique allowed us not only to reliably determine the oxidation state of sulfur from the binding energy (E_b) measured for the S 2p_{3/2} signal but also to reveal the component to which sulfur is bound. To solve the latter problem, we used a method based on the differential charging effect, the essence of which consists in different charging of test catalyst sample components (in this case, BaCO₃ and CeO₂) in the process of electron photoemission during the measurement of XPS spectra. As a result of differential charging, the same element (for example, sulfur), which occurs in the same oxidation

state but is the constituent of different components, appears in the spectrum as different signals on the scale of binding energies. Previously, this method was used in the analysis of the nature of nitrites and nitrates formed on the surface of a Pt/BaCO₃/Al₂O₃ model NSR catalyst upon its interaction with NO_x (a mixture of NO, O₂, and H₂O) [24].

EXPERIMENTAL

The experiments were performed using a VG ESCA-3 photoelectron spectrometer at a residual pressure of $<5 \times 10^{-7}$ Pa in the analyzer chamber. Non-monochromatic MgK_α radiation ($h\nu = 1253.6$ eV) was used to obtain the XPS spectra. Before the experiments, the binding energy scale of the spectrometer was calibrated using the following signal positions of gold and copper metals: Au 4f_{7/2} (84.0 eV) and Cu 2p_{3/2} (932.6 eV). The treatment of the photoemission spectra (the deconvolution into individual components, the measurement of XPS peak areas, and the determination of binding energies) of the test samples was performed after Shirley background subtraction.

The samples of a model NSR catalyst were prepared as a thin film on the surface of tantalum foil. To exclude the interaction of catalyst components with tantalum, the foil was coated with an aluminum oxide film ~100 Å in thickness by evaporation aluminum metal in an atmosphere of oxygen at 1.3×10^{-3} Pa before supporting the catalyst components. Barium carbonate and cerium dioxide were supported onto the surface of the alumina film from a suspension of BaCO₃ and CeO₂ (in a molar ratio of 1 : 1) in ethanol followed by drying in air and calcination in a vacuum at 600°C. The BaCO₃ and CeO₂ film thickness was sufficient for the complete shielding of signals from the Al₂O₃/Ta substrate in the measurements of XPS spectra. Then, platinum was supported by thermal evaporation in a vacuum. Previously, an analogous method was used for the preparation of model catalysts for XPS analysis [24].

The resulting model catalyst samples were treated with SO_x in a mixture of SO₂ (260 Pa), O₂ (2600 Pa), and H₂O (525 Pa) at 150 and 300°C with the subsequent regeneration in a mixture of CO (2100 Pa) and H₂O (525 Pa) at 500, 600, and 700°C in the preparation chamber of the spectrometer. The samples were heated by passing an alternating current through the tantalum foil. The temperature was measured using a Chromel-Alumel thermocouple welded to the reverse side of the foil. After each treatment in a reaction mixture, the sample was transferred to the analyzer chamber away from contact with the atmosphere for measuring the spectra.

Table 1. Binding energies in the XPS spectrum of the initial Pt/(BaCO₃ + CeO₂) sample obtained directly from the spectra and corrected for differential charging

Signal	Measured values of E_b , eV	Corrected values of E_b , eV		Assignment
		$\Delta_B = 6.7$ eV	$\Delta_C = 4.9$ eV	
C1s	291.5	284.8 (+)	—	C/Pt/BaCO ₃
	295.9	289.2 (+)	—	CO ₃ ²⁻ /BaCO ₃
O1s	535.2	528.5 (?)	530.3	O ²⁻ /CeO ₂
	538.0	531.3 (+)	—	CO ₃ ²⁻ /BaCO ₃
Ba3d _{5/2}	783.7	777.0 (?)	778.8	Ba ²⁺ /CeO ₂
	785.6	778.9 (+)	—	Ba ²⁺ /BaCO ₃
Ba4d _{5/2}	95.7	89.0 (+)	—	Ba ²⁺ /BaCO ₃
Ce3d, u"	921.6	914.9 (?)	916.7	Ce ⁴⁺ /CeO ₂
Ce4d, A	114.2	107.5 (?)	109.3	Ce ⁴⁺ /CeO ₂
Pt4f _{7/2}	76.8	70.1(?)	71.9	Pt/CeO ₂
	78.7	72.0(+)	—	Pt/BaCO ₃

RESULTS AND DISCUSSION

Analysis of the XPS Spectra of the Pt/(BaCO₃ + CeO₂) Catalyst in the Initial State

As mentioned above, during the recording of the XPS spectra of multicomponent systems, each of the test sample components acquires a stationary positive potential in the process of electron photoemission; in this case, as a rule, its values are different for different components. As a result, the photoemission signals of an element, which is the constituent of a certain component, is shifted from the true position by a value corresponding to the potential acquired by the given component. The internal standard method is the simplest method for the quantitative evaluation of potential and the determination of the true positions of binding energies of photoemission signals under conditions of the differential charging of the test sample [24, 25–27]. The C 1s signal from amorphous carbon, which is accumulated on the sample surface upon exposure to residual gases in the spectrometer chamber, is commonly used as an internal standard. The binding energy of this C 1s signal is taken to be 284.8 eV. Figure 1 shows the spectrum in the C 1s region of a sample of the Pt/(BaCO₃ + CeO₂) model catalyst in the initial state. The spectrum is the superposition of two signals with binding energies of 291.5 and 295.9 eV. Based on

the conditions of sample preparation, one of these signals with the greatest binding energy belongs to carbon as the constituent of carbonate ions in BaCO₃, whereas it is obvious that the other signal belongs to amorphous carbon.

By analogy with our previous work [24], we analyzed the binding energies (E_b) of signals in the XPS spectrum of an initial catalyst sample, which were obtained taking into account their shifts as a result of differential charging. Under the assumption that the C 1s signal with a binding energy of 291.5 eV belongs to amorphous carbon with the tabulated value of $E_b = 284.8$ eV, the shift is $\Delta_B = 6.7$ eV. Table 1 summarizes the values of E_b obtained directly from the spectra (column 2) and after correction for the differential charging Δ_B (column 3). The plausible values of binding energy are marked by a plus sign. The values that cannot be ascribed to a particular chemical compound are indicated by a question mark. Let us consider consecutively all of the E_b values given in Table 1 (column 3).

As mentioned above, two signals are observed in the spectrum of the C 1s region (Fig. 1); the most intense of these signals is attributed to amorphous carbon, and its binding energy of 284.8 eV specifies a charging value of 6.7 eV. The other signal after correction for charging acquires the value of $E_b = 289.2$ eV, which is

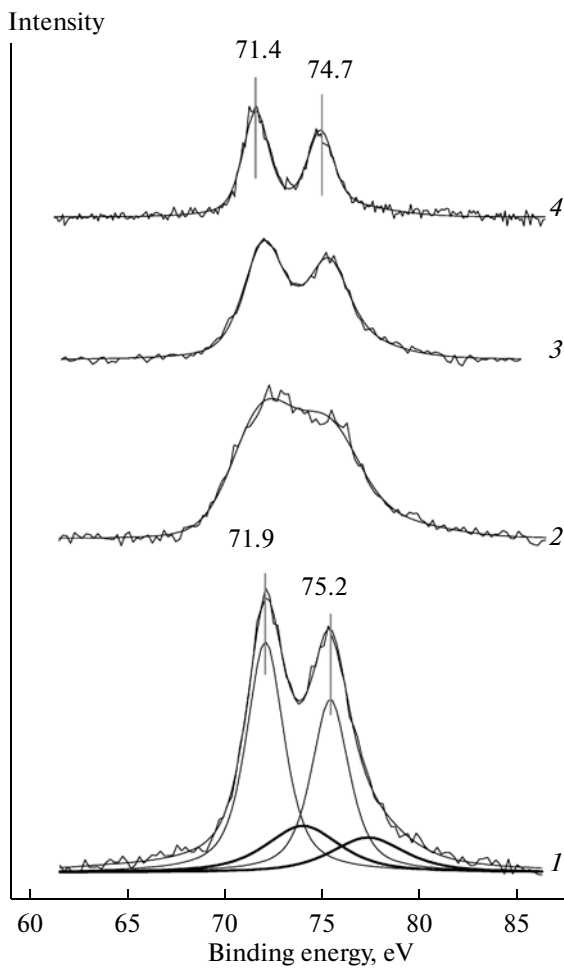


Fig. 2. XPS spectra of the Pt/(BaCO₃ + CeO₂) model catalyst measured in the Pt 4f region (1) in the initial state and (2) after its reaction with SO_x (260 Pa SO₂ + 2600 Pa O₂ + 525 Pa H₂O) at 300°C and the subsequent regeneration in a mixture of 2100 Pa CO + 525 Pa H₂O at (3) 500 or (4) 700°C.

characteristic of inorganic carbonates, in particular, BaCO₃ [24, 28–30]. In the O1s region, the spectrum is also the superposition of two signals with an intensity ratio of ~1 : 1 (Table 1). After correction for charging, the binding energy of one of the signals becomes 531.3 eV, which is close to the values published for barium carbonate (530.7–531.2 eV) [24, 28–30]. In this case, the second signal becomes 528.5 eV, which is substantially lower than the value expected for both BaCO₃ and CeO₂ (530.4 eV) [31]. In the Ba 3d and Ba 4d spectral regions, which characterize barium, signals are observed the binding energies $E_b(\text{Ba } 3d_{5/2})$ and $E_b(\text{Ba } 4d_{5/2})$ of which after correction for Δ_B acquire the values of 778.9 and 89.0 eV respectively, which will agree well with those published for barium carbonate [24, 28–30]. Thus, the use of the correction $\Delta_B = 6.7$ eV, which was obtained from the position of the C 1s signal of amorphous carbon, for determining true binding energies gives reasonable values for the C 1s (289.2 eV), O 1s (531.3 eV), Ba 3d_{5/2} (778.9 eV),

and Ba 4d_{5/2} (89.0 eV) signals, which can be related to one of the components in the model catalyst—BaCO₃.

At the same time, the correction for Δ_B gives too low values of binding energies for the signals that characterize cerium. Thus, according to published data for CeO₂, the signal u'' in the Ce 3d region has $E_b \approx 916.7$ eV [32–34] and the signal A in the Ce 4d region, ~109.3 eV [31]. For the second signal in the O1s region, the use of Δ_B as a correction also gives a binding energy 2 eV lower than that expected for CeO₂ [31]. A low-intensity signal detected in the Ba 3d region should also be noted. For this signal, the binding energy corrected for Δ_B is $E_b(\text{Ba } 3d_{5/2}) = 777.0$ eV; this anomalously low value was observed in none of barium compounds [35, 36]. All the above suggests that, indeed, the potential of CeO₂ differed from the potential of BaCO₃ in the course of XPS measurements; that is, differential charging occurred, and the C 1s signal of amorphous carbon cannot be used as an internal standard for CeO₂. A possible reason consists in an insignificant accumulation of amorphous carbon on the surface of CeO₂ because of a significant oxidizing power of the latter. For example, published survey spectra [37] indicate that carbon deposits were almost absent on the surface of a Ce-containing oxide. Thus, another signal suitable to serve as an internal standard should be found in the spectrum. It is most convenient to use the u'' signal for this purpose; in the complex Ce 3d spectrum, this signal is located separately from other signals and has a stable binding energy value of 917.6 eV [32, 34, 37, 38]. Taking into account this binding energy $E_b(u'')$, we obtain the correction $\Delta_C = 4.9$ eV for the CeO₂ component. Taking into account this correction, we calculated binding energies for all “strange” photoemission signals (the corresponding values are given in Table 1, column 4). It is evident that, after the correction for Δ_C , the signals occupy the expected positions. Moreover, a weak doublet signal observed as a shoulder in the Ba 3d spectrum acquires a value of $E_b = 778.8$ eV after correction for Δ_C ; this value is typical of barium in the oxidation state Ba²⁺. On this basis, this signal can be ascribed to barium cations in contact with CeO₂. A similar state of barium was found earlier in the Pt/BaCO₃/Al₂O₃ model catalyst and referred to Ba²⁺ cations located at the BaCO₃–Al₂O₃ interface [24].

After the establishment of the fact that two components (BaCO₃ and CeO₂) that acquire different positive potentials in the course of XPS measurements occur in the test model catalyst, let us discuss the spectra that characterize platinum supported onto the surface of these components. Figure 2 (curve 1) shows the Pt 4f spectrum of the initial catalyst. It is difficult to separate the individual signals that belong to platinum supported onto BaCO₃ and CeO₂ from the overall outline of the Pt 4f spectrum. Nevertheless, it is evident that the shape of the Pt 4f spectrum cannot be described by one Pt 4f_{7/2}–Pt 4f_{5/2} doublet. We attempted to decompose this spectrum into two doublets (Figure 2, spec-

trum 1), one of which (more intense with a smaller binding energy) can be related to platinum supported on CeO_2 and the other, which is less intense with a larger binding energy, to platinum on BaCO_3 . In this approach, the intensity ratio between the Pt 4f signals that characterize platinum on CeO_2 and BaCO_3 is 2.53, which practically coincides with the Ce : Ba atomic ratio (2.57) determined from Ce 3d and Ba 3d signal intensities. In Fig. 2, the spectra are shifted by the CeO_2 charging Δ_C along the axis of E_b ; therefore, the Pt 4f signal position of platinum supported on CeO_2 corresponds to the true binding energy $E_b(\text{Pt } 4f_{7/2})$, which is 71.9 eV for the initial sample (Table 1). Taking into account the charging Δ_B for the second signal, we obtained a similar value of $E_b(\text{Pt } 4f_{7/2}) = 72.0$ eV. Although the occurrence of platinum particles in a metal state is expected based on a vacuum evaporation procedure, the found binding energy $E_b(\text{Pt } 4f_{7/2})$ is higher than the corresponding value for bulk platinum—71.2 eV [35, 36]. The observed difference can be explained by the manifestation of the final state effect in the process of electron photoemission from the small (about several nanometers) particles of the supported metal [39–41]. Similar values of $E_b(\text{Pt } 4f_{7/2})$ we obtained earlier upon platinum evaporation onto the surfaces of Al_2O_3 [42] and $\text{BaCO}_3/\text{Al}_2\text{O}_3$ [24].

Table 1 (the last column) summarizes the assignment of all of the observed signals based on the corrected values of binding energies. From the standpoint of XPS, the model catalyst sample, which is schematically depicted in Fig. 3, consist of two subsystems: Pt/ BaCO_3 (subsystem B (based on BaCO_3)) and Pt/ CeO_2 (subsystem C (based on CeO_2)). Based on the intensities of photoemission signals with consideration for atomic sensitivity factors [35], we estimated the chemical composition of both of the subsystems:

$$\begin{array}{ll} \text{Pt}/\text{BaCO}_3 \text{ (subsystem B)} & \text{Ba : C : O} = 1 : 2.1 : 7.0, \\ \text{Pt}/\text{CeO}_2 \text{ (subsystem C)} & \text{Ce : O} = 1 : 2.5. \end{array}$$

The O : Ce ratio in CeO_2 higher than the stoichiometric ratio can be explained by the partial hydroxylation of the oxide surface. As judged from the atomic ratio between the elements in subsystem B, it is most likely that its surface layer consists of barium bicarbonate, $\text{Ba}(\text{HCO}_3)_2$. The platinum contents of subsystems B and C evaluated from the intensities of the corresponding Pt 4f, Ce 3d, and Ba 3d_{5/2} signals and expressed in terms of atomic ratios are the following:

$$\begin{array}{ll} \text{subsystem B} & \text{Pt : Ba} = 0.6 : 1, \\ \text{subsystem C} & \text{Pt : Ce} = 0.7 : 1. \end{array}$$

Interaction of Pt/(BaCO₃ + CeO₂) with SO_x

Figure 4 shows the S 2p spectra of the Pt/(BaCO₃ + CeO₂) catalyst recorded (1) before and after its treatment in a mixture of SO_x at (2) 150 and (3) 300°C. The

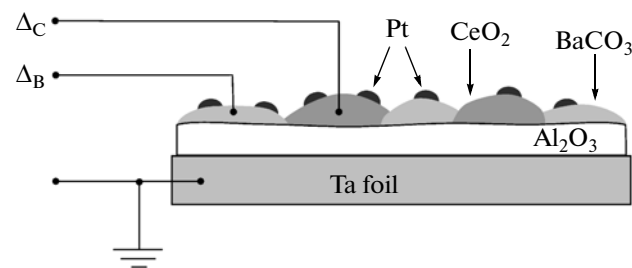


Fig. 3. Schematic diagram of the Pt/(BaCO₃ + CeO₂) model catalyst; Δ_B and Δ_C are positive charges acquired by the Pt/BaCO₃ and Pt/CeO₂ subsystems, respectively, as a result of electron photoemission in the course of XPS measurements.

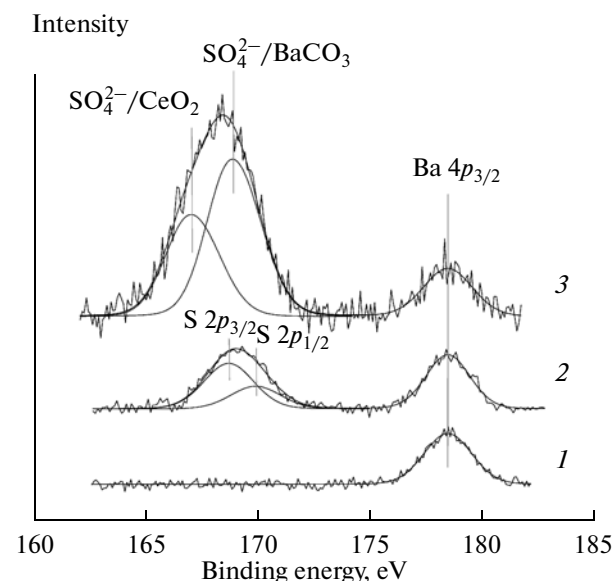


Fig. 4. XPS spectra of the Pt/(BaCO₃ + CeO₂) model catalyst measured in the S2p region (1) in the initial state and after its reaction with SO_x (260 Pa SO₂ + 2600 Pa O₂ + 525 Pa H₂O) at (2) 150 or (3) 300°C.

Ba 4p_{3/2} signal, which is also shown in the spectra in Fig. 4, was located closely to the S 2p signals. The position of this signal remains almost unchanged after treatment in SO_x; therefore, the accuracy of the determination of the binding energy of S 2p signals can be additionally controlled with respect to $E_b(\text{Ba } 4p_{3/2})$. After the interaction of the catalyst with SO_x at 150°C, a signal appeared in the S 2p region; this signal exhibited noticeable asymmetry because it is the S 2p_{3/2}–S 2p_{1/2} doublet with a spin–orbital splitting of 1.2 eV and an intensity ratio of 2 : 1 [35]. After correction for Δ_B , the binding energy $E_b(\text{S } 2p)$ acquires a value of 168.5 eV or, taking into account decomposition into spin–orbital components, $E_b(\text{S } 2p_{3/2}) = 169.1$ eV, which is typical of sulfur in inorganic sulfates. In particular,

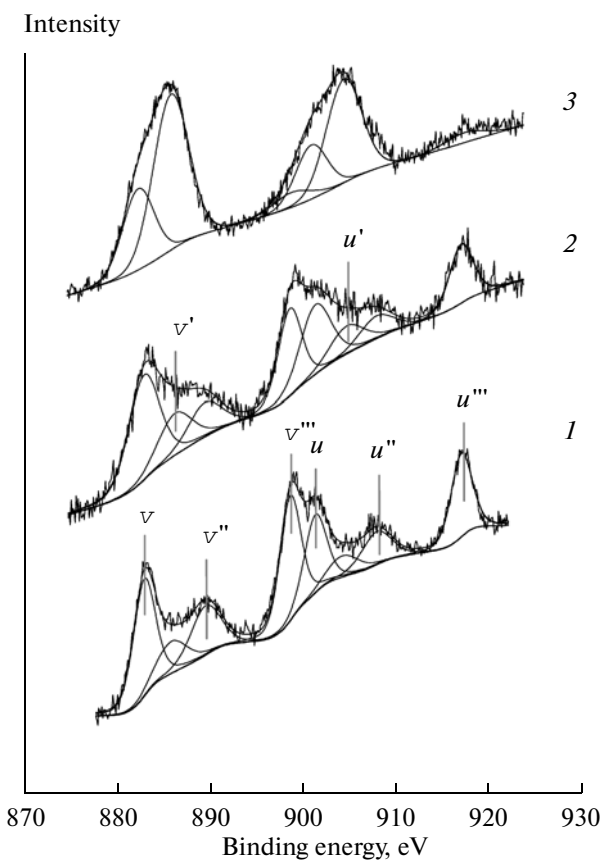


Fig. 5. XPS spectra of the Pt/(BaCO₃ + CeO₂) model catalyst measured in the Ce 3d region (1) in the initial state and after its reaction with SO_x (260 Pa SO₂ + 2600 Pa O₂ + 525 Pa H₂O) at (2) 150 or (3) 300°C.

Christie et al. [28] published the value of $E_b(S\ 2p) = 168.4$ eV for BaSO₄. If we determine $E_b(S\ 2p_{3/2})$ corrected for Δ_C in subsystem C (Pt/CeO₂), we obtain a value of 171.1 eV, which is too high to be ascribed to an oxygen compound of sulfur. Thus, the treatment of the model catalyst in SO_x at 150°C leads to the predominant formation of barium sulfate.

As the interaction temperature was increased to 300°C, the intensity of the S 2p signal increased. The simultaneous signal broadening and the appearance of a shoulder on the side of smaller E_b values indicate the formation of at least two S-containing compounds. After decomposing spectrum 3 in Fig. 4 into two components and shifting it by the differential charging Δ_B along the axis of binding energies, we can see that one of the components should be attributed to barium sulfate. The S 2p signal intensity of BaSO₄ substantially increases in comparison with the signal intensity after treatment in SO_x at 150°C. The binding energy $E_b(S\ 2p_{3/2})$ of the second component acquires a value of 167.9 or 169.1 eV with the chosen correction Δ_B or Δ_C , respectively. The former value can correspond to sulfite ions in the composition of the Ba-containing component (subsystem B), whereas the latter value

can correspond to sulfate ions as the constituents of the Ce-containing component (subsystem C).

The Ce 3d spectra recorded in the course of treatment of the model catalyst in SO_x (Fig. 5) suggest that the discussed S 2p signal belongs to particles of the sulfate nature. Spectrum 1 of the catalyst in the initial state has a shape characteristic of cerium dioxide. The spectrum has a complex structure formed by the superposition of three Ce 3d_{5/2}—Ce 3d_{3/2} doublet signals [32, 38, 43] inherent to Ce⁴⁺ cations, which appear because of the fact that cerium cations can relax into different final states after electron photoemission from the Ce 3d level [44]. In the spectrum of the initial catalyst in Fig. 5, these signals are designated by the symbols v, v'', and v''' for Ce 3d_{5/2} or u, u'', and u''' for Ce 3d_{3/2}, respectively, in accordance with the designations proposed by Burroughs et al. [43]. The doublet marked by the symbols v' and u' was related to electron photoemission from the Ce³⁺ cation [32–34, 37, 38]. The Ce³⁺ content of the initial catalyst was 15%, as determined from the intensity ratio between signals that form the Ce 3d spectrum; this value is consistent with estimations published for cerium oxides [45]. The detection Ce³⁺ in an amount of 10–20% in the XPS spectra of CeO₂ was usually related to the partial reduction of the CeO₂ under the action of X-radiation or as a result of the reaction with residual gases (CO and H₂) [34, 46]. After the interaction with SO_x at 150°C, the structure of the Ce 3d spectrum did not crucially change; the contribution of Ce³⁺ remained at almost the same level (~18%). After the interaction at 300°C, the spectrum changed dramatically to acquire a shape typical of Ce(III) compounds [31, 34]. The change in the structure of the Ce 3d spectrum, which suggests the reduction of Ce(IV) to Ce(III) in parallel with the appearance of the S 2p signal with a binding energy characteristic of sulfates in the Pt/CeO₂ subsystem, is a convincing argument in favor of the formation of Ce(III) sulfate at 300°C. Previously, we obtained cerium sulfate by the interaction of the CeO₂ [38] and Pt/CeO₂ [47] model systems with SO₂ and a mixture of SO₂ + O₂ in the temperature range of 200–400°C.

In Fig. 2, spectrum 2 in the Pt 4f region was obtained after the interaction of the catalyst with SO_x at 300°C. A considerable broadening of signals was observed, as compared with the spectra of samples in the initial state. For this reason, it becomes impossible to separate two doublets that characterize platinum supported separately onto BaCO₃ and CeO₂. Nevertheless, we can reliably state that $E_b(Pt\ 4f_{7/2})$ did not strongly change after treatment in SO_x; that is, platinum remained in a metal state. Indeed, the oxidation of supported platinum particles upon the interaction of the Pt/BaCO₃/Al₂O₃ model catalysts with NO_x resulted in a shift of the Pt 4f spectrum to the region of higher binding energies by 1–1.5 eV [24, 42], which

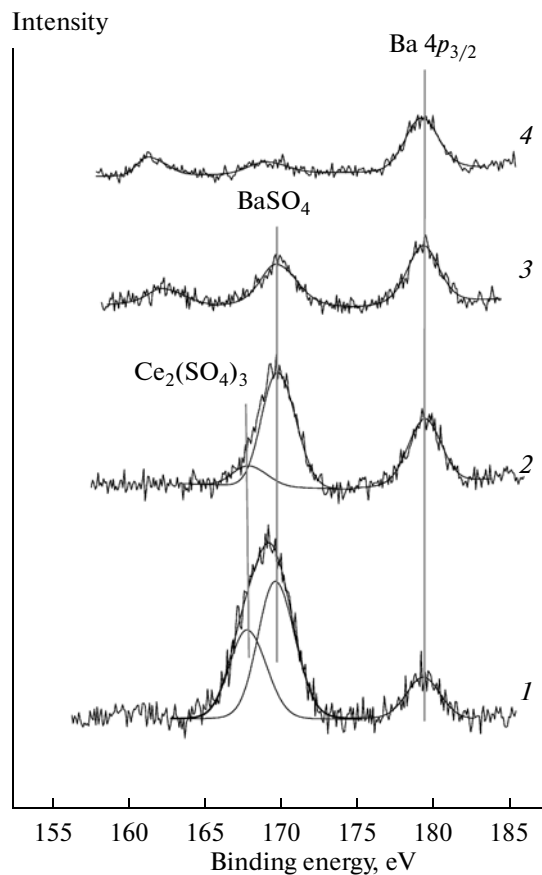


Fig. 6. XPS spectra of the Pt/(BaCO₃ + CeO₂) model catalyst measured in the S 2p region (*1*) after its reaction with SO_x (260 Pa SO₂ + 2600 Pa O₂ + 525 Pa H₂O) at 300°C and the subsequent regeneration in a mixture of 2100 Pa CO + 525 Pa H₂O at (2) 500, (3) 600, or (4) 700°C.

was not the case in the spectra depicted in Fig. 2. It should be noted that changes in $E_b(\text{Pt } 4f_{7/2})$ were also not observed in a study of the interaction of platinum supported on Al₂O₃ or CeO₂ with SO_x (SO₂ + O₂) in the temperature range of 30–400°C [47].

Regeneration of the Pt/(BaCO₃ + CeO₂) Catalyst after Sulfatization

Figure 6 shows the S 2p spectra recorded (*1*) after the interaction of the Pt/(BaCO₃ + CeO₂) catalyst with SO_x at 300°C and in the course of the subsequent regeneration in a mixture of CO and H₂O at (2) 500, (3) 600, and (4) 700°C. As demonstrated in the previous section, barium and cerium sulfates were present on the catalyst surface after sulfatization. Two S 2p signals spaced at ~2 eV on the binding energy scale in spectrum 2 correspond to the above sulfates because of the different charging of the Pt/BaCO₃ and Pt/CeO₂ subsystems. After the treatment of the sulfated catalyst in a mixture of CO and H₂O at 500°C, the major portion of cerium sulfate disappeared, whereas the

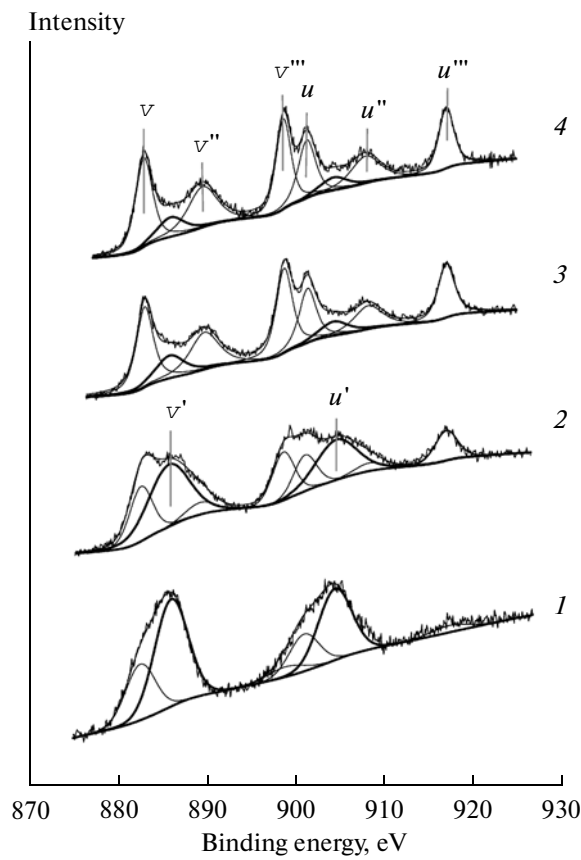


Fig. 7. XPS spectra of the Pt/(BaCO₃ + CeO₂) model catalyst measured in the Ce 3d region (*1*) after its reaction with SO_x (260 Pa SO₂ + 2600 Pa O₂ + 525 Pa H₂O) at 300°C and the subsequent regeneration in a mixture of 2100 Pa CO + 525 Pa H₂O at (2) 500, (3) 600, or (4) 700°C.

decomposition of barium sulfate occurred to an insignificant degree. The decomposition of cerium sulfate was accompanied by the appearance of signals characteristic of the state Ce(IV) in the Ce 3d spectrum and a decrease in the intensity of signals due to Ce(III) (Fig. 7, spectrum 2). Table 2 summarizes the S : Ba and S : Ce atomic ratios calculated for sulfate ions bound in Ba and Ce sulfates, respectively, and the contribution (on a percentage basis) of the Ce(III) state to the Ce-containing component. The conversion of Ce(III) into Ce(IV) under the action of a reducing atmosphere (CO) seems unusual; nevertheless, this observation can be explained taking into account the fact that the SO₄²⁻ anions can serve as an oxidant for both Ce³⁺ and carbon monoxide:



The possibility in principle for the occurrence of this reaction at elevated temperatures follows from the estimated isobaric-isothermal potential of the reaction determined from thermodynamic parameters [48, 49] with no regard for the temperature dependence of heat capacities. At room temperature (298 K), $\Delta G_{298}^0 \approx$

Table 2. S : Ba and S : Ce atomic ratios and the percentage concentration of Ce(III) as a constituent of a catalyst sulfated at 300°C in the course of its regeneration in a mixture of CO and H₂O at different temperatures

Sample	S O ₄ ²⁻ /Ba	S O ₄ ²⁻ /Ce	Ce(III), %
Initial catalyst	—	—	15.5
After interaction with SO _x at 300°C	0.97	0.80	(Ce ₂ O ₃)
After interaction with CO + H ₂ O			
at 500°C	0.79	0.12	34
at 600°C	0.41	—	11
at 700 °C	0.11	—	10

154 kJ/mol, whereas this value becomes negative at 500°C (773 K): $\Delta G_{773}^0 \approx -87$ kJ/mol.

An increase in the reaction temperature to 600 and then to 700°C led to the complete decomposition of cerium sulfate (Fig. 6, Table 2) and, as judged from the Ce 3d spectrum (Fig. 7), the regeneration of cerium in the Ce(IV) state. Barium sulfate is more stable: a considerable decrease in the intensity of its S 2p signal occurs in the course of interaction over the temperatures range of 600–700°C (Fig. 6, Table 2). Starting with a temperature of 600°C, an additional signal in the region of smaller binding energies appeared in the S 2p spectrum. With consideration for the correction Δ_B for charging, $E_b(S\ 2p)$ was 162.0 eV for the interaction temperature of 600°C or 160.8 eV for 700°C. With consideration for the correction Δ_C , $E_b(S\ 2p)$ became 163.1 eV for 600 or 162.2 eV for 700°C. All of the obtained values of binding energy fall within the range characteristic of bulk metal sulfides. In particular, the values of 161.5–162.0 and 163.6 eV were reported for BaS [50, 51] and PtS [52], respectively. The value of $E_b(S\ 2p)$ in the range of 162.2–162.5 eV was obtained for surface platinum sulfide, which was formed upon the interaction of supported platinum catalysts with SO₂ or H₂S [47, 53]. Thus, we can convincingly state that sulfides are formed in the process of the reducing regeneration of the sulfated catalyst. However, at the same time, it is very difficult to unambiguously identify the resulting sulfides (BaS, PtS) based on only the binding energies $E_b(S\ 2p)$ even taking into account differential charging.

Previously, it was reported that the conversion of sulfates into barium sulfide occurs in the process of the reducing regeneration of NSR catalysts [8, 10, 12, 13]. At the same time, in a number of cases, the formation of platinum sulfide was also assumed [4, 10, 14, 15]. It is well known that the conversion of platinum into the PtS sulfide is accompanied by an increase in the binding energy $E_b(Pt\ 4f_{7/2})$ by ~1.5 eV, as compared with that of platinum metal [53]. As can be seen in Fig. 2

(spectra 3 and 4), on the contrary, upon the interaction of the catalyst with a mixture of CO + H₂O at 500 and 700°C, the binding energy $E_b(Pt\ 4f_{7/2})$ decreased by ~0.5 eV, as compared with that of the initial sample, to acquire a value close to that of the state of bulk platinum metal. Thus, in the case under consideration, the formation of platinum sulfide under the conditions of reducing regeneration is not confirmed. When the NSR catalyst contained CeO₂ and the treatment of the catalyst in SO_x led to the formation of cerium(III) sulfate, reducing procedures can lead to the formation of Ce(III) oxo sulfide, Ce₂O₂S [54]. Spectra 3 and 4 in Fig. 7 and data given in the last column of Table 2 indicate that, in the case under consideration, regeneration almost completely converted cerium into the Ce(IV) state; therefore, the conversion of cerium sulfate into sulfide did not occur. Thus, based on the above facts, being it is most reasonable to ascribe the S 2p signal with a binding energy of 161–162 eV, which appeared after the reducing regeneration of the catalyst sample at high temperatures, to the barium sulfide BaS.

Thus, using the Pt/(BaCO₃ + CeO₂) model NSR catalyst as an example, we demonstrated the applicability of the differential charging effect in the measurement of X-ray photoelectron spectra to the identification of compounds formed on the surface of a multi-component catalyst upon its interaction with a reaction atmosphere. We found that barium sulfate was predominantly formed in the reaction of the catalyst with SO_x (SO₂ + O₂ + H₂O) at 150°C. An increase in the reaction temperature to 300°C resulted in the additional formation of cerium sulfate, which was accompanied by the reduction of Ce(IV) to Ce(III). Supported platinum particles retained their metal state in the course of reaction with SO_x. The regeneration of the catalyst sulfated at 300°C in a mixture of CO and H₂O caused the decomposition of cerium(III) sulfate at temperatures of ≤500°C. In spite of the presence of a strong reducing agent (CO) in the reaction atmosphere, the decomposition of cerium sulfate was accompanied by the oxidation of surface Ce(III) cat-

ions to CeO_2 . At treatment temperatures of $\leq 500^\circ\text{C}$, the major portion of barium sulfate was retained. The decomposition of BaSO_4 was observed in the temperatures range of $600\text{--}700^\circ\text{C}$, and it was accompanied by the formation of an amount of the sulfide BaS .

REFERENCES

1. Matsumoto, S., *Cattech*, 2000, vol. 4, p. 102.
2. Epling, W.S., Campbell, L.E., Yezerets, A., Currier, N.W., and Parks, J.E., *Catal. Rev.*, 2004, vol. 46, p. 163.
3. Breen, J.P., Marella, M., Pistarino, C., and Ross, J.R.H., *Catal. Lett.*, 2002, vol. 80, p. 123.
4. Sedlmair, C., Seshan, K., Jentis, A., and Lercher, J.A., *Catal. Today*, 2002, vol. 75, p. 413.
5. Liu, Z. and Anderson, J.A., *J. Catal.*, 2004, vol. 228, p. 243.
6. Rohr, F., Peter, S.D., Lox, E., Kogel, M., Sassi, A., Juste, L., Rigaudeau, C., Belot, G., Gelin, P., and Primet, M., *Appl. Catal., B*, 2005, vol. 56, p. 201.
7. Wei, X., Liu, X., and Deeba, M., *Appl. Catal., B*, 2005, vol. 58, p. 41.
8. Elbouazzaoui, S., Corbos, E.C., Courtois, X., Marecot, P., and Duprez, D., *Appl. Catal., B*, 2005, vol. 61, p. 236.
9. Anderson, J.A., Liu, Z., and Garcia, M.F., *Catal. Today*, 2006, vol. 113, p. 25.
10. Abdulhamid, H., Fridell, E., Dawody, J., and Skoglundh, M., *J. Catal.*, 2006, vol. 241, p. 200.
11. Strehlau, W., Leyrer, J., Lox, E.S., Kreuzer, T., Hori, M., and Hoffmann, M., *SAE Technical Paper*, 1996, no. 962047.
12. Poulston, S. and Rajaram, R.R., *Catal. Today*, 2003, vol. 81, p. 603.
13. Kim, D.H., Scanyi, J., Kwak, J.H., Szailer, T., Hanson, J., Wang, C.M., and Peden, C.H.F., *J. Phys. Chem. B*, 2006, vol. 110, p. 10 441.
14. Limousy, L., Mahzoul, H., Brilhae, J.F., Garin, F., Maire, G., and Gilot, P., *Appl. Catal., B*, 2003, vol. 45, p. 169.
15. Fridell, E., Amberntsson, A., Olsson, L., Grant, A.W., and Skoglundh, M., *Top. Catal.*, 2004, vols. 30–31, p. 143.
16. Ji, Y., Toops, T.J., and Crocker, M., *Catal. Lett.*, 2009, vol. 127, p. 55.
17. Matsumoto, S., Ikeda, Y., Suzuki, H., Ogai, M., and Miyoshi, N., *Appl. Catal., B*, 2000, vol. 25, p. 115.
18. Yamazaki, K., Suzuki, T., Takahashi, N., Yokota, K., and Sugiura, M., *Appl. Catal., B*, 2001, vol. 30, p. 459.
19. Fanson, P.T., Horton, M.R., Deglass, W.N., and Lauterbach, J., *Appl. Catal., B*, 2003, vol. 46, p. 393.
20. Basile, F., Fornasari, G., Grimandi, A., Livi, M., and Vaccari, A., *Appl. Catal., B*, 2006, vol. 69, p. 58.
21. Corbos, E.C., Elbouazzaoui, S., Courtois, X., Bion, N., Marecot, P., and Duprez, D., *Top. Catal.*, 2007, vols. 42–43, p. 9.
22. Corbos, E.C., Courtois, X., Bion, N., Marecot, P., and Duprez, D., *Appl. Catal., B*, 2008, vol. 80, p. 62.
23. Phatak, A.A., Koryabkina, N., Rai, S., Ratts, J.L., Ruettiger, W., Farrauto, R.J., Blau, G.E., Deglass, W.N., and Ribeiro, F.H., *Catal. Today*, 2007, vol. 123, p. 234.
24. Smirnov, M.Yu., Kalinkin, A.V., Dubkov, A.A., Vovk, E.I., Sorokin, A.M., Nizovskii, A.I., Carberry, B., and Bukhtiyarov, V.I., *Kinet. Katal.*, 2008, vol. 49, p. 876 [*Kinet. Catal. (Engl. Transl.)*, vol. 49, p. 831].
25. Bukhtiyarov, V.I., Prosvirin, I.P., and Kvon, R.I., *J. Electron Spectrosc. Relat. Phenom.*, 1996, vol. 77, p. 7.
26. Bukhtiyarov, V.I., Prosvirin, I.P., Kvon, R.I., Goncharova, S.N., and Bal'zhinimaev, B.S., *J. Chem. Soc., Faraday Trans.*, 1997, vol. 93, p. 2323.
27. Jaramillo, A., Spurlock, L.D., Young, V., and Brajter-Toth, A., *Analyst*, 1999, vol. 124, p. 1215.
28. Christie, A.B., Lee, J., Sutherland, I., and Walls, J.M., *Appl. Surf. Sci.*, 1983, vol. 15, p. 224.
29. Teterin, Yu.A. and Sosulinikov, M.I., *Physica C*, 1993, vol. 212, p. 306.
30. Miot, C., Husson, E., Proust, C., Erre, R., and Coutreras, J.P., *J. Mater. Res.*, 1997, vol. 12, p. 2388.
31. Mullins, D.R., Overbury, S.H., and Huntley, D.R., *Surf. Sci.*, 1998, vol. 409, p. 307.
32. Romeo, M., Bak, K., El Fallah, J., Le Normand, F., and Hilaire, L., *Surf. Interface Anal.*, 1993, vol. 20, p. 508.
33. Hardacre, H., Roe, G.M., and Lambert, R.M., *Surf. Sci.*, 1995, vol. 326, p. 1.
34. Park, P.W. and Ledford, J.S., *Langmuir*, 1996, vol. 12, p. 1794.
35. Moulder, J.F., Stickle, W.F., Sobol, P.E., and Bomben, K.D., *Handbook of X-Ray Photoelectron Spectroscopy*, Eden Prairie, Minn.: PerkinElmer, 1992.
36. Nefedov, V.N., *Rentgenoelektronnaya spektroskopiya khimicheskikh soedinenii* (X-Ray Photoelectron Spectroscopy of Chemical Compounds), Moscow: Khimiya, 1984.
37. Smirnov, M.Yu. and Graham, G.W., *Catal. Lett.*, 2001, vol. 72, p. 39.
38. Smirnov, M.Yu., Kalinkin, A.V., Pashis, A.V., Sorokin, A.M., Noskov, A.S., Kharas, K.C., and Bukhtiyarov, V.I., *J. Phys. Chem. B*, 2005, vol. 109, p. 11712.
39. Huizinga, T., van't Blik, H.F.J., Vis, J.C., and Prins, R., *Surf. Sci.*, 1983, vol. 135, p. 580.
40. Parmigiani, F., Kay, E., Bagus, P.S., and Nelin, C.J., *J. Electron Spectrosc. Relat. Phenom.*, 1985, vol. 36, p. 257.
41. Steinrück, H.-P., Pesty, F., Zhang, L., and Madey, T.E., *Phys. Rev. B: Condens. Matter*, 1995, vol. 51, p. 2427.
42. Smirnov, M.Yu., Kalinkin, A.V., and Bukhtiyarov, V.I., *Zh. Strukt. Khim.*, 2007, vol. 48, p. 1120 [*J. Struct. Chem. (Engl. Transl.)*, vol. 48, p. 1053].
43. Burroughs, P., Hamnett, A., Orchard, A.F., and Thornton, G., *J. Chem. Soc., Dalton Trans.*, 1976, p. 1686.
44. Fujimori, A., *Phys. Rev. B: Condens. Matter*, 1983, vol. 28, p. 2281.

45. Shyu, J.Z., Weber, W.H., and Gandhi, H.S., *J. Phys. Chem.*, 1988, vol. 92, p. 4964.
46. Paparazzo, E., *Surf. Sci.*, 1990, vol. 234, p. L253.
47. Smirnov, M.Yu., Kalinkin, A.V., Pashis, A.V., Sorokin, A.M., Noskov, A.S., Bukhtiyarov, V.I., Kharas, K.S., and Rodkin, M.A., *Kinet. Katal.*, 2003, vol. 44, p. 629 [*Kinet. Catal. (Engl. Transl.)*, vol. 44, p. 575].
48. *Svoistva neorganicheskikh soedinenii: Spravochnik* (Properties of Inorganic Compounds: A Handbook), Efimov, A.I., Belorukova, L.P., Vasil'kova, I.V., and Chechey, V.P., Eds., Leningrad: Khimiya, 1983.
49. *Khimicheskaya entsiklopediya* (Encyclopedia of Chemistry), Moscow: Bol'shaya Rossiiskaya Entsiklopediya, 1995, vol. 4.
50. Rohr, F., Gobel, U., Kattwinkel, P., Kreuzer, T., Muller, W., Philipp, S., and Gelin, P., *Appl. Catal., B*, 2007, vol. 70, p. 189.
51. Stakheev, A.Yu., Gabrielsson, P., Gekas, I., Teleguina, N.S., Bragina, G.O., Tolkachev, N.N., and Baeva, G.N., *Top. Catal.*, 2007, vols. 42–43, p. 143.
52. Visser, J.P.R., Groot, C.K., van Oers, E.M., de Beer, V.H.J., and Prins, R., *Bull. Soc. Chim. Belg.*, 1984, vol. 93, p. 813.
53. Wang, T., Vazques, A., Kato, A., and Schmidt, L.D., *J. Catal.*, 1982, vol. 78, p. 306.
54. Luo, T., Vohs, J.M., and Gorte, R.J., *J. Catal.*, 2002, vol. 210, p. 397.